J Math Chem (2010) 47:29–40
DOI 10.1007/s10910-009-9527-3

ORIGINAL PAPER

Studies on the effects of nonadiabatic behavior during the course of HBr photolysis

Dongfang Zhang

Received: 15 December 2008 / Accepted: 21 January 2009 / Published online: 27 March 2009

Abstract From quantum mechanical simulation, photodissociation of hydrogen bromide (HBr) in its first UV absorption continuum (*A* band) taking place upon excitation has been studied. The absorbencies are inferred from techniques of Forurier transformation. On that foundation, the branching fractions for the spin-excited $Br^*(^2P_{1/2})$ channel at enormous photon frequencies are gained. Moreover, the relevant MOs have been analyzed to obtain more information about the dissociation process within the framework of the time-dependent density functional theory. The results unravel that the possibility of intersystem crossing does exist in the photodissociation course, which involve the coupling of the $a^3\Pi_0{}^+$ and $A^1\Pi_1$ potential surfaces. The prediction of the wavelength dependence of the anisotropy parameter β agrees with the experiment within a major part of *A* band, which provides an insight into the reaction dynamics and the transiton probability is conjectured to be larger when channels approach each other, notwithstanding a steady decline towards the red wing of spectrum.

Keywords Nonadiabatic behavior · Photolysis · Angular distribution

1 Introduction

Up to now, intense efforts have been made to develop strategies [1–13] to deal with the energy flow involving two or more adiabatic states. Ordinarily, molecular systems are simulated on a classical computer to uncover the importance of flux transfer in chemical and biological systems [14,15], which in conjunction with semiclassical computations can yield rational results [16,17]. This method is more appealing than the direct quantum approach in two ways: (1) it is generally easily to apply, and (2)

D. Zhang (✉)
College of Science, Huazhong Agricultural University, Wuhan 430070, People's Republic of China
e-mail: zdfbubai@yahoo.com

it presents a simpler and clearer picture of the photodissociation process and hence lends more physical diagnosis into the mechanism of switching surfaces. Lately, the photodissociation of HBr has become the issue of a variety of study because bromine atoms are estimated to be 40 times as efficient as chlorine atoms at destroying stratospheric ozone on an atom-for-atom basis [18] and the ensemble of diatomic have long been viewed as the prototypical systems to enhance our in-depth understanding of the photochemical reaction [19,20]. Investigations on the unimolecular photodissociation such as H_2O, H_2S, HCl and their homologues [21–25] are ample and have revealed that nonadiabatic curve crossing effects play an intricate role in the fragmentation processes. Undoubtedly, detailed knowledge of the electronic states accessed in the initial photoexcitation and subsequent irreversible evolution is indispensable to discover the underlying mechanism behind the system fully.

There has been substantial attention in the photodissociation of HBr molecules. Magnotta et al. [26] have measured the relative yield of the Br atoms in the ground ($^2P_{3/2}$) and excited ($^2P_{1/2}$) states following photoexcitation in 193 nm, while other groups [27–30] exploited the laser-based techniques involving Doppler spectroscopy to measure the relative yield for photodissociation of HBr at 193 and 243 nm. The precedents indicate that the ratio of the final populations in the two fine structure levels decreases with the increase of excitation wavelength. Shortly thereafter, some experiments [31–33] have utilized fixed-frequency ultraviolet lasers to study these processes, and then it has been possible to start studying the energy dependence of the branching fraction and angular distribution. These works has focused on measuring two paramount identities: (1) the branching fraction ρ, which provides the yield of spin–orbit (SO) excited atoms $Br^*(^2P_{1/2})$ relative to the total yield, and (2) the anisotropy parameter β, which provides information on the parallel or perpendicular nature of the electronic transitions contributing to the dissociation. Through the determination of these properties, the roles of the multiple electronic states and the possible nonadiabatic coupling can be determined. To this end, exploring the mechanism of hydrogen bromide photolysis is required since the quantum flux transfer via surface hopping approach usually has an inevitable influence on the yields of the final products.

The main goal of the present work is to describe a computational assessment of the first absorption band of Hbr, and the nonadiabatic transition probability is compared with the experimental value estimated from the beta parameter. The elastic scattering is treated by a sophisticated semiclassical analysis, and the Landau–Zener model is postulated to be valid for illuminating the trends in photodissociation. The switching amplitude (or probability) of the $a^3\Pi_0{}^+$ and $A^1\Pi_1$ states is extracted by virtue of one-dimensional Landau–Zener manner. The crossing effects are hence capable of providing valuable information on the unimolecular eliminiation.

2 General methods

The dissociation of the title system can be tackled by using the one-dimensional time dependent Schrödinger equation

$$i\hbar\frac{\partial\psi(R,t)}{\partial t} = [\hat{U}(R) + \hat{T}(R)]\psi(R,t) \tag{1}$$

where R is the nuclear coordinate, $T(R)$ and $U(R)$ are the nuclear and electronic parts of total molecular Hamiltonian, respectively and $\psi(R, t)$ is the dissociative wave function.

The initial wave packets $\psi(R, t = 0)$ are builted via the vibrational eigenstate $\varphi(R)$ of the electronic ground state multiplied by the appropriate transition dipole functions [34]

$$\psi_n(R, t = 0) = T_n(R)\varphi(R) \tag{2}$$

where the subscript n indicates the wave packet on the potential corresponding to the electronic state (n) and $T_n(R)$ is the associated transition moment.

The short time step split-operator scheme is used to propagate the wave train: $\psi(R, t) = \exp(-i\hat{H}t/\hbar)\phi(R, t = 0)$. For a Δt time step this propagator is given by

$$\begin{aligned}\exp\left(-i\frac{\hat{H}}{\hbar}\Delta t\right) \approx \exp\left(-i\frac{\hat{T}}{2\hbar}\Delta t\right)\exp\left(-i\frac{\hat{U}}{\hbar}\Delta t\right)\\ \times \exp\left(-i\frac{\hat{T}}{2\hbar}\Delta t\right)\end{aligned} \tag{3}$$

The photodissociation information are extracted at an analysis line fixed at $R = R_\infty$. Energy dependent amplitudes $\gamma_n(R_\infty, E)$ are expressed as

$$\gamma_n(R_\infty, E) = \frac{1}{2\pi}\int_0^\infty \psi_n(R_\infty, t)\exp[i(E_0 + h\omega)t/\hbar]dt \tag{4}$$

where E_0 being the energy of initial state, ω is the photon frequency, and R_∞ is a parameter that is chosen to be large enough that at $R \geq R_\infty$ the PES becomes flat. The extinction coefficient ε is given as

$$\varepsilon_n(\omega) = \frac{32\pi\omega k_n}{3c\varepsilon_0}|\gamma_n(R_\infty, E)|^2 \tag{5}$$

where k_n is the asymptotic wave vector for the nth channel.

In order to avoid unphysical reflection, the wave packet is smoothly cut off at the edges of the grid area. Thus, the wave packet vector should multiplied by a damping function at each time step to absorb its scattered parts before it arrives at the boundaries of grid. The form of the absorbing potential (L_{abs}) are defined by

$$L_{\text{abs}}(R) = 1.0 \quad \text{If } R < R_0 \tag{6a}$$

$$L_{\text{abs}}(R) = \exp(-L_{\text{opt}} \cdot \Delta t)[(R - R_0)/(R_{\max} - R_0)]^{3/2} \quad \text{Otherwise} \tag{6b}$$

where R_0 is the point where the damping is switched on and the parameter L_{opt} is chosen in such a way that the effect of the reflection and transmission is minimised. The computations are executed by *Fortran V6.1 code*, from which the parameters employed are outlined in Table 1. The potential curves are derived by using the molcas 5.4 suite of programs [35]. The starting guess on the orbitals are made firstly

Table 1 Input parameters to perform the time-dependent wave packet calculation

Variable	Description	Value
Atomic masses	μ_{H}	1.0079 amu
	μ_{Br}	79.904 amu
Reduced mass	μ	1814.61 a.u.
Range of grid	$R_{\min}$, $R_{\max}$	1.0–12.0 a_0
Number of equidistant points		2048
Position of r_∞		9.00 a_0
Time step	Δt	0.483776 fs
Number of time steps		8192
Start of absorbing region	R_0	9.50 a_0
Decay factor	L_{opt}	0.015 fs^{-1}

by using the spin-restricted Hartree–Fock (RHF) method. Then the state-averaged *casscf* calculations are carried out, taking the previous RHF orbitals as starting values for orbital optimization. The selected active space comprises eight electrons spread over six orbitals, which includes two extra nonvalence orbitals that obtained from the initial RHF calculations, the H–Br σ and σ^* orbitals, and the two 4p orbitals of bromine. Utilizing the previous CAS(8e/6o) energies as reference values, the energies of the $\Lambda-$S states are computed. The new relativistic basis sets of the atomic natural orbital type, ANO-RCC [36], which are contracted to 3s2p1d and 6s5p3d2f1g, respectively, are used for hydrogen and bromine atoms.

3 Results and discussion

The calculated adiabatic potential curves for the low-lying valence states are shown in Fig. 1. The $X^1\Sigma_0{}^+$ ground state of HBr is characterized by a $[..]\sigma^2\pi^4\sigma^{*0}$ valence electron configuration, where π MO is dominated by the p-orbital of bromine. Apart from the $X^1\Sigma_0{}^+$ state is the only one among the valence states possessing a strongly bound characteristic and it converges to the lowest Br $(^2P_{3/2}) + \mathrm{H}(^2S_{1/2})$ dissociation limit. The next four valence electronic states are dissociated to the $^2P(\mathrm{Br}\,4p) + {}^2S(\mathrm{H}\,1s)$ atomic state. Expansion of the molecular wavefunction for the states involved over the atomic basis will reveal the following asymptotic ($R \to \infty$) correlations: $a^3\Pi_1 \to |1/2\,1/2;\,3/2\,1/2|$, $A^1\Pi_1 \to |1/2\,-1/2;\,3/2\,3/2|$ and $t^3\Sigma_1{}^+ \to |1/2\,1/2;\,1/2\,1/2|$. Since transitions between states are governed by selection laws and Franck–Condon factor, many of the Ω states are not readily accessible. Taking into account the Hund's case (c), the allowed transitions for a one photon process are determined by the following selection rules: $\Delta\Omega = 0, \pm 1$; $0^+ \leftrightarrow 0^+$; $0^- \leftrightarrow 0^-$ and thus the transitions to the $\Omega = 1$ state should be accessed through configuration mixing. An aspect that is not present in lighter systems involves the Br-atom excited SO level, $^2P_{1/2}$, whose electron density is nearly spherical [37]. Because the SO energy is large (i.e., 3685 cm^{-1}) [38], the $^2P_{1/2}$ spherical electron density remains reasonably robust down to the short H–Br distances, i.e., relative to light halogens. Consequently, the Br* $(^2P_{1/2})$ atom couples weakly with the H atom, resulting in a shallow van der Waals-type minimum. Said differently, strong SO coupling inhibits the participation of "traditional" bonding

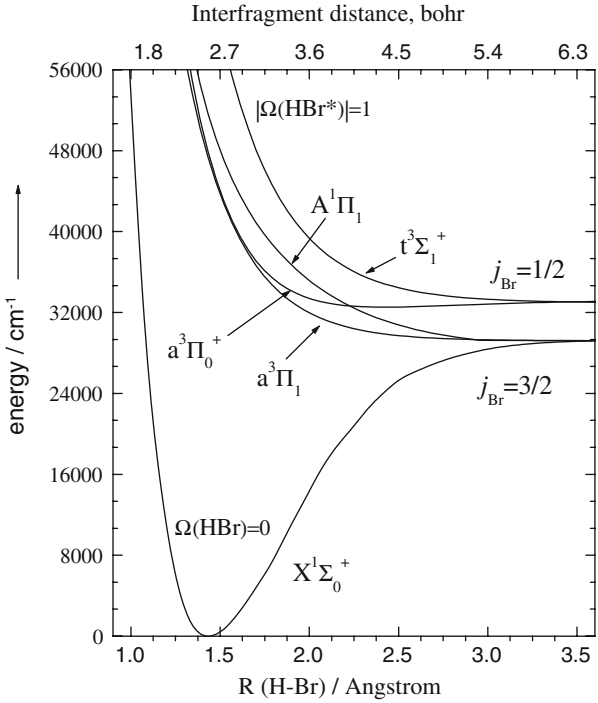

Fig. 1 One-dimensional potential cuts along the H–Br bond for the low-lying states

and antibonding molecular orbitals. This and other relativistic effects has been uncovered in the analogous system such as the isoelectronic HI molecule [39], which is particularly difficult for heavy elements that display a variety of bonding interactions due to the many chemically accessible valence orbitals. The molecular constants computed for the ground state are in agreement with the available experimental [33,40] results. The dissociation energy of the ground state $D_0(\mathrm{X0}^+)$ can be estimated from the average energy of the three Ω states converging to the lowest Br $(^2P_{3/2})+\mathrm{H}(^2S_{1/2})$ atomic limit at $R = 12.0\,\mathrm{a_0}$, the largest internuclear separation treated in the present study. This gives $D_0(\mathrm{X0}^+) = 29292\,\mathrm{cm}^{-1} = 3.632\,\mathrm{eV}$, which agrees well with the experimental value of 3.745 eV [33]. It is worth noting that the accuracy of the ground state potential in the FC region is better than the bonding strength value, which should allow a fairly reliable calculation of the absorption spectrum, and the SO coupling on the ground state equilibrium distance and vibrational frequency can be overlooked, because this effect is marginal and changes quite slowly near the equilibrium distance [34]. Thereby the calculations have captured the most important elements of these interactions. The results for the oscillator strengths, f, a unitless quantity which is used to bridge the classical and quantum mechanical descriptions for an oscillating electron interacting with light are given in Table 2. Having in mind that the higher valence $\mathrm{t}^3\Sigma_1{}^+$ state still retains some characters of Rydberg progressions converging to the vibrational states of the ion, which may present a bottleneck that undergo

Table 2 Parameters describing the ground and valence states of HBr

Electronic state	Vertical energies T_0 (eV)	Oscillator strengths (f)	Coefficients and ingredients
$a^3\Pi_1$	6.054	0.001	$17\pi \rightarrow 19\sigma^*$, 0.7287
$a^3\Pi_0{}^+$	6.172	0.0003	$18\pi \rightarrow 19\sigma^*$, 0.7805
$A^1\Pi_1$	6.941	0.0021	$17\pi \rightarrow 19\sigma^*$, 0.6875
$t^3\Sigma_1{}^+$	8.833	0.0001	$16\sigma \rightarrow 19\sigma^*$, 0.7676

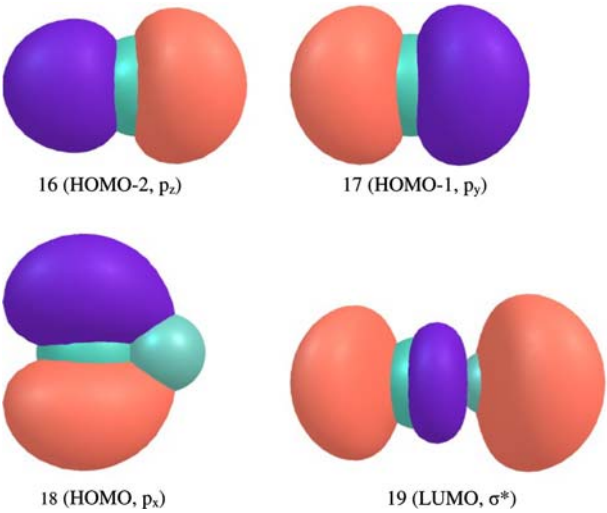

Fig. 2 The boundary surface density plots of relevant MOs of HBr calculated at the TD-B3pw91/cc-pVTZ level

light-induced transformation. At this point, the initial transition relevant to the *A* band precludes the possibility of wave packet mapped onto the $t^3\Sigma_1{}^+$ surface.

It is now general wisdom that high-level methods such as augmented correlation consistent triple-zeta (cc-pVTZ) basis sets advocate the possibility to obtain accurate energies, whereby the ab initio calculations are taken to probe the decay channels that linked to the low-lying excited states of HBr, and the pertinent molecular orbitals have been examined without indicating the positions of the Br and H nuclei. Figure 2 shows the three highest occupied molecular orbitals (HOMO) and the lowest unoccupied orbital (LUMO) with their related bonding nature, which are computed at the TD-B3pw91/cc-pVTZ level (the orientation of H–Br bond is tagged with Z-axis for labeling of the p orbitals). Explicitly, the p lone-pair orbitals of the bromine atoms, which are represented in the atomic orbital (AO) basis, can be partitioned into the standard energetically highest occupied MOs and constitute the key origin for the formation of the low-lying excited states, where the electrons of each MO are migrated only into the virtuals of the fragment to which they belong. The computed $a^3\Pi_1$, $A^1\Pi_1 \leftarrow X$ transition is essentially a promotion of a p electron from the nonbonding π(HOMO-1) orbital to the front virtual (external) MOs and the other

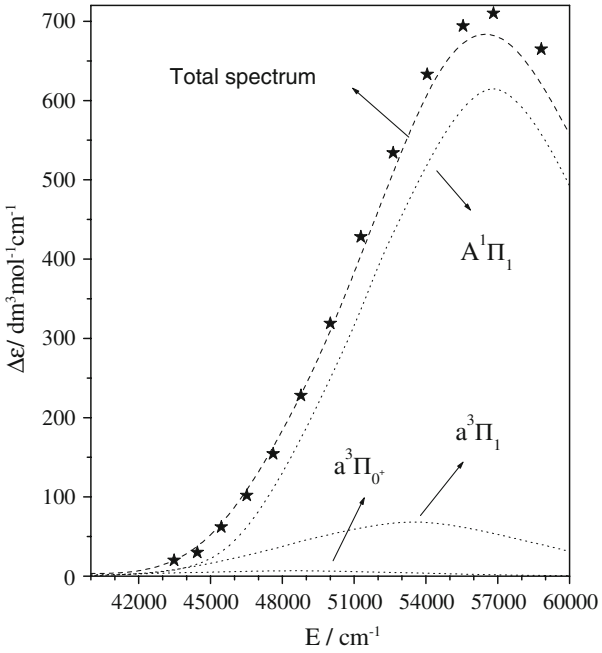

Fig. 3 The partial and total absorption spectrum for a part of the *A*-band in HBr photolysis: *dotted line*—calculated value; Pentagonal *Star*—experimental data

two excited states $a^3\Pi_0{}^+$ and $t^3\Sigma_1{}^+$ are also correlate to the p electron in the two energetically occupied MOs transit to the σ^*_{H-Br}, and imagined to correlate with H–Br bond cleavage.

To obtain the absorption feature of the molecular photodecay, the numerical principle is implemented in the present simulation. For one-photon transition, the packets are anticipated to born on a series of dissociative surface by pumping pulse. The extinction coefficients ε ($dm^3\,mol^{-1}\,cm^{-1}$) for transitions from the $X^1\Sigma_0{}^+$, $\nu'' = 0$ to the A-band states are determined, which alongside the total absorption spectra are shown in Fig. 3. The shapes of the spectra depend mainly on two factors: (1) the position and size of the Franck–Condon windows on the potential curves for the initial excitation and (2) the dynamics of the wave packet. Therefore, the transitions reflect only the dynamics of the wave packets in the individual Franck–Condon windows, opened by the excitation. In Fig. 3, the onset for the *A*-band absorption (here is taken as a formal starting point $\varepsilon = 0.58\,dm^3\,mol^{-1}\,cm^{-1}$) occurs at about $39700\,cm^{-1}$, at which energy excitation to the $a^3\Pi_1$ state dominates the absorption. It can be seen that the absorption curves of $a^3\Pi_1$ and $A^1\Pi_1$ states are somewhat broad and flat, with maxima at 53472 and $56870\,cm^{-1}$, respectively. Thus it is argued that these two states will play a crucial role on the photodissociation event. Alternatively, the gas-phase absorption spectrum [41] of HBr is displayed in the same panel. It can be recognized that the crude shape of the absorption spectrum is diffuse without any spikes. Instead of the theoretical treatments reconcile to the reported data, there are slight discrepancy in the magnitude of total intensity near the intermediate region of the *A* spectrum band.

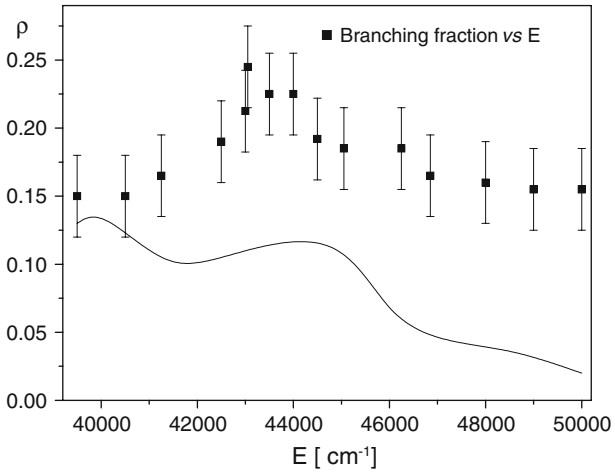

Fig. 4 The outcomes of the calculations of Br* branching fractions (*solid line*) in comparison with the exact sources of data points (*squares* with error bars) of product branching in photodissociation event

The extinction intensity is calculated to be $\varepsilon \approx 686\,\mathrm{dm^3\,mol^{-1}\,cm^{-1}}$ at $56818\,\mathrm{cm^{-1}}$, while the systematic error can be missed except for the visible deficiency emerged in the range of 55556–58823 $\mathrm{cm^{-1}}$. The overall absorption profile of the simulated spectrum resembles that of the experimental data evince the quantitative information can be obtained, especially in the red side of the *A* band.

Among the three states discussed, $\mathrm{a^3\Pi_1}$ and $\mathrm{A^1\Pi_1}$ dissociate to the Br ($^2P_{3/2}$) limit, conversely, $\mathrm{a^3\Pi_0{}^+}$ go to the Br* ($^2P_{1/2}$) spin-excited asymptote. Since the impact of nonadiabatic effects remains not very sure on the yields of photodissociation products, the present $\rho(\nu)$ branching fraction for the channel H+Br* ($^2P_{1/2}$) can be determined efficaciously by taking the ratio of the extinction coefficients

$$\rho(\nu) = \frac{\varepsilon[a^3\Pi_0{}^+]}{\varepsilon[A^1\Pi_1] + \varepsilon[a^3\Pi_1] + \varepsilon[a^3\Pi_0{}^+]} \tag{7}$$

at all relevant frequencies.

The computed $\rho(\nu)$ branching fraction for the photon-induced dissociation of HBr from its lowest vibrational state and the literature values [42] are exhibited in Fig. 4. It can be detected that the agreement between the calculated and experimental branching fraction as a function of photolysis energy is not well and the right order of magnitude of former is in conflict with the experimental observations, which reflecting the theoretical yields for product channel H+Br* that has been estimated in the present work, which is expressed in the adiabatic approximation, is simply incorrect. Notwithstanding the relative weights for transitions to the electronic states with the Br* ($^2P_{1/2}$) dissociation asymptote is small, however, the initial transition to the $\mathrm{A^1\Pi_1}$ states perhaps have some influence on the $\rho(\nu)$ values for $E > 42 \times 10^3\,\mathrm{cm^{-1}}$, and this effect can be induced by the nonadiabatic transfer of quantum flux from the initial populated $\mathrm{A^1\Pi_1}$ state to the $\mathrm{a^3\Pi_0{}^+}$ state. In the following, we contemplate

that these sort of state-to-state transitions occur effectively in molecular dynamics process to cause the redistribution of quantum flux, and if it is true, we can quite safely guess that surface-hopping are involved in these processes. In order to assess the action that nonadiabatic mechanism takes, the crossing behavior is described with recourse to the Landau–Zener model [43,44], and an attempt is made to extract the crossing probability touching to the angular distributions. In a photodissociation process, angular distribution $F(\Theta)$ of the fragment can be obtained by integrating the reconstructed three-dimensional spatial distribution over a proper range of speed at each angle. It may be characterized by an anisotropy parameter, β, as expressed by [45]

$$F(\Theta) = (4\pi)^{-1}[1 + \beta P_2(\cos\Theta)] \tag{8}$$

where $\beta(-1$ to $2)$ is the observed anisotropy parameter because of the small alignment effects, Θ is the angle that fragment ejection direction relative to the laser polarization since the center-of-mass beam velocity not changed during the bond scission. The parameter β can be determined by fitting Br* angular distributions with functional form of $F(\Theta)$, and it can be drawn that

$$\chi = \frac{2-\beta}{2(1+\beta)} \tag{9}$$

where χ represents the weighting factor of perpendicular component, which is identical to the fraction of Br* fragments via the pure crossing between the $A^1\Pi_1$ and $a^3\Pi_0{}^+$ surface in the chosen basis. Therefore, the crossing probability P_0, for Br reverts to Br* is written as

$$P_0 = \frac{\chi\varepsilon[\mathrm{tot}]\rho(\nu)}{\varepsilon[A^1\Pi_1]} \tag{10}$$

where ε[tot] is the total extinction intensity. Factually, the prerequisite of aforementioned theory is dynamic mechanism arising from the coupling matrix element in the diabatics, which merely could be sparked by the intersystem crossing. The concept of Landau–Zener model entails the description of the nonadiabatic mechanism happens, that is, the crossing behavior should not violate the Landau–Zener criterion. By the same token, the nature of curve crossing can be rationally clarified. The transition probability for one passage of a crossing point in this case is given by

$$P_t = 1 - \exp(-\alpha/u_f) \tag{11}$$

where u_f stands for the recoil velocity of cofragments at the crossing point. The impact parameter α is related to the gradients of two potential curves at the crossing radius and independent of excitation energy, which can be viewed as invariance. As envisioned, the crossing takes place at the position of $R_{cc} = 2.208$ Å and energy at this point is $32626.9\,\mathrm{cm}^{-1}$. If P_0 follows from the LZ formula, the identity $\ln(1 - P_0) = -\alpha/u_f$ should be satisfied, and the variation of probability P_0 relative to the recoil velocity u_f

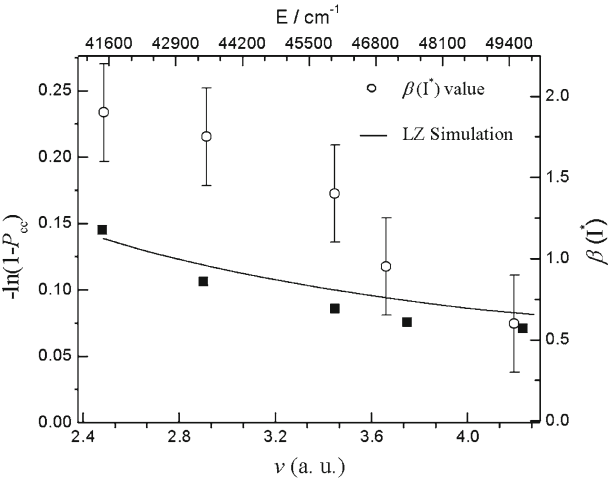

Fig. 5 The beta parameter β plotted as a function of photon energies and a Landau–Zener description for crossing dynamics. The error bars indicate an uncertainty for one standard deviation

will be guided by the impact parameter α, which are functions of the phase difference $\Delta\eta$, between the decay fluxing on the $a^3\Pi_0{}^+$ and $A^1\Pi_1$ states.

It is gratifying to see from Fig. 5 that the agreement of the Landau–Zener prediction with the experimental phenomena as a function of dissociation wavelength is excellent and hence exemplified the goodness of fit. According to the popular semiclassical theory, the optical absorption causes a change of electronic state of the molecule and it is assumed due to Franck–Condon rule that there is no change in the geometry of the system. Then the system can propagate on the surface of the given state to its minimum or to encounter another state, singlet or triplet. Then the systems can nonadiabatically transfer from one state to another if there is a crossing between them. Needless to say, the avoided crossing exists if the involved states belongs to the similar reflection symmetry, or else it is circumvented when the reflection symmetry with respect to xz plane is diverse. In the former case the internal conversion can take place, while the intersystem crossing takes place in the latter case, which ought to readily driven by vibronic SO coupling and vice versa. If the original trajectory splits into two branch trajectories. The upper branch will proceed on $a^3\Pi_0{}^+$ surface while the lower branch proceeds on $A^1\Pi_1$ surface. The upper branch is created by a local electronic transition, wherein the nuclear coordinates are continuous. However, there is a discontinuity in nuclear kinetic energy equal to the energy difference between the surfaces at the transition point. Thus there is no unique platform to redistribute this energy difference among the various components of nuclear momentum on $a^3\Pi_0{}^+$ surface. A transition then occurs smoothly at an intersection point so that nuclear momenta as well as nuclear coordinates are continuous through the transition point. In practice the trajectory of outgoing flux need not pass through the intersection point itself, but must simply go over the point. So that an intersection point is equivalent to a branch point and going over the point is tantamount to crossing a branch cut. In view of these, the fact that crossing behavior obeys the L–Z formula convincingly hints that

the possibility of nonadiabatic mechanism (namely, surface hopping) induced by the coupling between two diabatic states ($a^3\Pi_0{}^+$ and $A^1\Pi_1$) cannot be omitted, and confer the importance of the nonadiabatic mechanism to the *A*-band photofragmentation.

4 Conclusions

The photofragmentation of HBr is examined by performing electronic structure calculations and simulation techniques. The molar extinction coefficients and final product state population are obtained by the numerical calculations, which exhibit a good agreement with the previous experimental results. The crossing behavior is simulated by using the Landau–Zener model, which reproduces the experimental findings that angular distribution changes as a function of photon energies accurately. The results indicate that photolysis proceeds with nonadiabatic mechanism between the $a^3\Pi_0{}^+$ and $A^1\Pi_1$ potentials and nonadiabatic curve crossing is of certain importance in the course of photodissociation within the *A*-band continuum.

References

1. R. Vetter, Chem. Phys. **343**, 303 (2008)
2. S.A. Vázquez, E. Martínez-Núñez, Chem. Phys. **349**, 219 (2008)
3. R. Schinke, S.Y. Grebenshchikov, Chem. Phys. **347**, 279 (2008)
4. D. Ewa, G. Ireneusz, U. Jacek, S. Jerzy, P. Jan, Chem. Phys. **348**, 249 (2008)
5. D.M.P. Holland, A.W. Potts, L. Karlsson, I.L. Zaytseva, A.B. Trofimov, J. Schirmer, Chem. Phys. **352**, 205 (2008)
6. M. Lewin, J. Math. Chem. **44**, 967 (2008)
7. P. Cassam-Chenaï, F. Patras, J. Math. Chem. **44**, 938 (2008)
8. B.I. Zhilinskiı́, J. Math. Chem. **44**, 1009 (2008)
9. B.T. Sutcliffe, J. Math. Chem. **44**, 988 (2008)
10. R. Sever, C. Tezcan, M. Aktas, Ö. Yesiltas, J. Math. Chem. **43**, 845 (2008)
11. C. Berkdemir, A. Berkdemir, R. Sever, J. Math. Chem. **43**, 944 (2008)
12. R. Sever, M. Bucurgat, C. Tezcan, Ö. Yesiltas, J. Math. Chem. **43**, 749 (2008)
13. M. Aktas, R. Sever, J. Math. Chem. **43**, 92 (2008)
14. L.J. Butler, Annu. Rev. Phys. Chem. **49**, 125 (1998)
15. F.S. Rowland, Annu. Rev. Phys. Chem. **42**, 731 (1991)
16. J. Zhang, H. Deng, J. Math. Chem. **43**, 12 (2008)
17. J.R. Laing, T.F. George, I.H. Zimmermann, Y.-W. Lin, J. Chem. Phys. **63**, 842 (1975)
18. A. Komornicki, T.F. George, K. Morokuma, J. Chem. Phys. **65**, 48 (1976)
19. S.C. Wofsy, M.B. McElroy, Y.L. Yung, Geophys. Res. Lett. **2**, 215 (1975)
20. J. Zoval, V. A. Apkarian, J. Phys. Chem. **98**, 7945 (1994)
21. R. Zadoyan, J. Almy, V.A. Apkarian, Faraday Discuss. **108**, 255 (1997)
22. Z. Xu, B. Koplitz, C. Wittig, J. Phys. Chem. **92**, 5518 (1988)
23. J.G. McCaffrey, H. Kunz, N. Schwentner, J. Chem. Phys. **96**, 155 (1992)
24. R. Zadoyan, Z. Li, C.C. Martens, V.A. Apkarian, J. Chem. Phys. **101**, 6648 (1994)
25. D. Zhang, Chem. Phys. **353**, 87 (2008)
26. F. Magnotta, D.J. Nesbitt, S.R. Leone, Chem. Phys. Lett. **83**, 21 (1981)
27. T. Kinugawa, T. Arikawa, J. Chem. Phys. **96**, 4801 (1992)
28. J. Park, Y. Lee, G.W. Flynn, Chem. Phys. Lett. **186**, 441 (1991)
29. P.M. Blass, R.C. Jackson, J.C. Polanyi, H. Weiss, J. Chem. Phys. **94**, 7003 (1991)
30. R. Liyanage, Y.-an Yang, S. Hashimoto, R.J. Gordon, R.W. Field, J. Chem. Phys. **103**, 6811 (1995)
31. S.R. Langford, P.M. Regan, A.J. Orr-Ewing, M.N.R. Ashfold, Chem. Phys. **231**, 245 (1998)
32. H.M. Lambert, P.J. Dagdigian, M.H. Alexander, J. Chem. Phys. **108**, 4460 (1998)
33. P.M. Regan, S.R. Langford, A.J. Orr-Ewing, M.N.R. Ashfold, J. Chem. Phys. **110**, 281 (1999)

34. D. Zhang, A. Abdel-Hafiez, B. Zhang, Chem. Phys. Lett. **428**, 49 (2006)
35. K. Andersson, M.P. Fulscher, R. Lindh, P.-Å. Malmqvist, J. Olsen, A.J. Sadlej, P.-O. Widmark, *MOLCAS version 5.4* (University of Lund, Lund, 2000)
36. B.O. Roos, R. Lindh, P.-L. Malmqvist, V. Veryazov, P.-O. Widmark, J. Phys. Chem. A **108** 2851 (2004)
37. M. Weissbluth, *Atoms and Molecules* (Academic Press, New York, 1978)
38. C.E. Moore, *Atomic Energy Levels* (U.S. Government Printing Office, Washington, DC, 1971)
39. N. Balakrishnan, A.B. Alekseyev, R.J. Buenker, Chem. Phys. Lett. **341**, 594 (2001)
40. K.P. Huber, G. Herzberg, *Molecular Spectra and Molecular Structure IV. Constants of Diatomic Molecules* (Van Nostrand, Princeton, 1979)
41. B.J. Huebert, R.M. Martin, J. Phys. Chem. **72**, 3046 (1968)
42. P.M. Regan, S.R. Langford, A.J. Orr-Ewing, M.N.R. Ashfold, J. Chem. Phys. **110**, 281 (1999)
43. E.E. Nikitin, *Theory of Elementary Atomic and Molecular Processes in Gases* (Oxford, New York, 1974), p. 107
44. D. Zhang, A. Abdel-Hafiez, B. Zhang, Chem. Phys. **342**, 119 (2007)
45. R.N. Zare, Mol. Photochem. **4**, 1 (1972)